Journal of King Saud University – Science 31 (2019) 804–812

Contents lists available at ScienceDirect

Journal of King Saud University – Science

journal homepage: www.sciencedirect.com

Thermal radiation on unsteady electrical MHD flow of nanofluid over stretching sheet with chemical reaction

Yahaya Shagaiya Daniel [a,b,1], Zainal Abdul Aziz [a,b,*], Zuhaila Ismail [a,b,1], Faisal Salah [c]

[a] Department of Mathematical Sciences, Faculty of Science, Universiti Teknologi Malaysia, 81310 UTM Johor Bahru, Johor, Malaysia
[b] UTM Centre for Industrial and Applied Mathematics, Universiti Teknologi Malaysia, 81310 UTM Johor Bahru, Johor, Malaysia
[c] Department of Mathematics, Faculty of Science, University of Kordofan, Elobied 51111, Sudan

ARTICLE INFO

Article history:
Received 21 August 2017
Accepted 11 October 2017
Available online 16 October 2017

Keywords:
MHD nanofluid
Thermal radiation
Chemical reaction
Electric field
Suction

ABSTRACT

This paper focuses on the effects of suction as well as thermal radiation, chemical reaction, viscous dissipation and Joule heating on a two-dimensional natural convective flow of unsteady electrical magnetohydrodynamics (MHD) nanofluid over a linearly permeable stretching sheet. One significant aspect of this study is that electric field employed in revised Buongiorno model has been introduced in view of enhancement of thermal conductivity and consequently better convective heat transfer. The constitute governing equations have been converted into strong non-linear ordinary differential equations by employing suitable transformations and these transformed equations are solved by the Implicit finite difference. From this study, it is found that the presence of magnetic field and suction slows down the fluid motion while it enhances for higher values of an electric field which tends to firmness sticky effect. It is also found that enhancing thermal radiation leads to an increase in nanofluid temperature. The Nusselt number increases with both Brownian motion and unsteadiness parameters.

1. Introduction

In recent times, Magnetohydrodynamics (MHD) boundary layer flow and heat transfer of electrically conducting fluids have various science, engineering and industrial applications include petroleum industries, crystal growth, geothermal engineering, nuclear reactors, liquid metals, aerodynamics and metallurgical processes (Hsiao, 2016; Khan et al., 2016, 2017c; Ullah et al., 2017; Makinde et al., 2017, 2016; Makinde and Animasaun, 2016; Ibrahim and Makinde, 2016; Hayat et al., 2017e, 2016b; Daniel, 2015c). Considering the effects of natural convective heat transfer occurrences tangled usually in the fields of science and engineering with relevant applications to geothermal systems, solar energy collectors, space technology, cooling of electronic equipment, lubricants, cooling of nuclear reactors etc (Sheikholeslami et al., 2016; Sheremet et al., 2016; Hayat et al., 2016a, 2017d, 2017c; Daniel, 2015a,b). Natural convection against permeable media has been employed for chemical catalytic, insulation for buildings, grain storage, reactors etc. Advanced kinds of fluid were required to meet up with the demands and expectations for more efficient performance in devices. Nanofluid was proposed a new kind of fluid to improve the thermal conductivity and convective heat transfer. This is achieved through ultrafine composed of nanoparticles of size 1–100 nm dispersed in a convention fluid (Choi and Eastman, 1995; Sharma et al., 2019). This fascinating features of kind of fluid known as nanofluids play a remarkable role in convective heat transfer processes. A novel kind of fluid should be interchanged as a replacement for of common working fluid. The virtue of enhanced thermal conductivity, nanofluids can be regarded as the best for heat transfer agents to pure fluid due to unpredictable enhancement (Kasaeian et al., 2017; Tamoor et al., 2017; Hayat et al., 2016c,g). Consequently, this draws the attention of various researchers to the analysis of convective boundary layer flow and heat transfer in nanofluids highly (Sheikholeslami and Ganji, 2017; Nayak et al., 2017; Waqas et al., 2016; Ahmed et al., 2019; Daniel et al., 2017c,b,a; Daniel, 2016a). Buongiorno (2006) developed a unique analytical model for the convective transport

* Corresponding author at: UTM Centre for Industrial and Applied Mathematics, Ibnu Sina Institute for Scientific and Industrial Research, 81310 UTM Johor Bahru, Johor, Malaysia.
E-mail addresses: shagaiya@kasu.edu.ng (Y.S. Daniel), zainalaz@utm.my (Z.A. Aziz), zuhaila@utm.my (Z. Ismail), faisal19999@yahoo.com (F. Salah).
[1] UTM Centre for Industrial and Applied Mathematics, Ibnu Sina Institute for Scientific and Industrial Research, 81310 UTM Johor Bahru, Johor, Malaysia.
Peer review under responsibility of King Saud University.

Production and hosting by Elsevier

https://doi.org/10.1016/j.jksus.2017.10.002
1018-3647/

Nomenclature

B_0	magnetic field
B	applied magnetic field
c_f	skin friction coefficient
D_B	Brownian diffusion coefficient
D_T	thermophoresis diffusion coefficient
E_0	electric field factor
E_1	electrical field parameter
E	applied electric field
Ec	Eckert number
$f\prime$	dimensionless velocity
Gr	Grashof number
Gm	mass Grashof number
$\bar{J}$	Joule current
k_1	rate of chemical reaction
$k,$	thermal conductivity
k_f, k_p	thermal conductivity of the base fluid and nanoparticle
M	magnetic field parameter
Nb	Brownian motion parameter
Nt	thermophoresis parameter
Nu	Nusselt number
Pr	Prandtl number
q_m	wall mass flux
q_r	radiative heat flux
q_w	wall heat flux
Rd	radiation parameter
Re	local Reynolds number
T	temperature
T_0	reference temperature
T_W	surface temperature at the wall
T_∞	ambient temperature
u, v	velocity component along $x-$ and $y-$ direction
u_W	stretching velocity
$\bar{V}$	velocity fluid
v_W	wall mass transfer

Greek symbols

$\sigma*$	Steffan-Boltzmann constant
σ	electrical conductivity
δ	unsteadiness parameter
η	dimensionless similarity variable
μ	dynamic viscosity of the fluid
υ	kinematic viscosity of the fluid
ρ	density
ρ_p	particle density
$(\rho)_f$	density of the fluid
$(\rho c)_f$	heat capacity of the fluid
$(\rho c)_p$	effective heat capacity of a nanoparticle
ψ	stream function
φ	concentration of the fluid
φ_0	reference concentration
φ_W	nanoparticle volume fraction at the surface
φ_∞	ambient concentration
θ	dimensionless temperature
ϕ	dimensionless concentration
τ	ratio between the effective heat transfer capacity and the heat capacity of the fluid
τ_W	surface shear stress
γ	chemical reaction parameter

Subscripts

∞	condition at the free stream
W	condition at the wall/surface

phenomena in nanofluid by considering Brownian motion and thermophoresis effects. Several authors have studied the problem of MHD boundary layer flow, heat and mass transfer about different surface geometries in electrically conducting fluids. Influence of Lorentz forces on nanofluid flow motion and thermal radiation (Sheikholeslami, 2017; Biglarian et al., 2017; Sheikholeslami and Shamlooei, 2017; Pal and Mandal, 2017; Khan and Azam, 2017; Daniel et al., 2017d; Daniel and Daniel, 2015; Daniel, 2016b). Radiative heat transfer is crucial due to remarkable applications includes power generation, nuclear reactor cooling, and combustion (Nayak et al., 2017; Hayat et al., 2017b; Sheikholeslami and Shehzad, 2017; Hayat et al., 2017a, 2016e; Daniel et al., 2017e). Such influences largely happened when the dissimilarity between the surface and ambient temperature is enormous, mostly in space vehicle re-entry, astrophysical flows, fossil fuel, solar power technology etc. Good insight of the processes involved in solar radiation has vital roles in the design of innovative energy conversion systems achieved at the advanced temperature (Sheikholeslami and Rokni, 2017; Waqas et al., 2017).

The chemical reaction stimulus a great role in the investigation involving heat and mass transfer in areas of science and engineering technology as result of wide coverage of industrial applications (Hayat et al., 2016d). It is deliberated to be essential as results of its key role in the design of chemical processing equipment, polymer production, cooling towers, pollution, creation and distribution of fog, temperature and fibrous insulation, etc (Khan et al., 2017a,b; Hayat et al., 2017f,h). Raw materials are built to go through the chemical reaction in industrial chemical practices to transform economy raw materials into advanced standard produces such as oxidation and synthesis of constituents, destruction of crops as results of cold, processing of food, moisture dispersal on cultivated fields, etc. Such chemical transformations are performed in a reactor. A chemical reaction between the conventional liquid and nanoparticles are classified as a homogeneous reaction during a given phase or heterogeneous reaction that is surrounded by a boundary of the phase. Reaction rate in a first-order chemical reaction is straightly related to the concentration. In view of the pertinent applications, several authors have considered and produced their results on chemical reaction effects on the flow of heat and mass transfer with different geometries (Hayat et al., 2016f, 2017g; Pontes et al., 2019).

The main aim here is to investigate the unsteady hydromagnetic natural convective flow of a revised nanofluid bounded by a linearly stretching sheet with an electric field. Flow analysis is investigated through permeable linear sheet which is imperiled to a transverse magnetic field normal to the plate. Brownian motion and thermophoresis are developed in energy and concentration expressions with chemical reaction. The boundary condition is passively controlled rather than active (Kuznetsov and Nield, 2013) with base fluid water (Mabood et al., 2015). Natural convection flow phenomenon has been studied in view of thermal radiation, viscous dissipation, and Joule heating as well as chemical reaction with the effect of suction considering passively flow behavior; this variation has not been considered by previous investigators. Hence, the motivation of this paper is to bridge this knowledge gap. The governing mathematical systems are

supplementary compound and linear in the frame of unsteady natural convection impacts. The arising mathematical modeling is scrutinized through the implementation of implicit finite difference scheme. The nonlinear ordinary differential systems of equations are computed with the sundry parameters. The nanofluid velocity, thermal and nanoparticle concentration fields are presented graphically and in tabular form in view of a number of governing parameters. Representation of skin friction coefficient and local Nusselt number are addressed through numerical values. It is hoped that the achieved results based on the computational scheme will not only provide valuable information for applications but also serve as a foundation for studying other related systems in engineering and industrial applications such as in polymer, food processing technology, and chemical manufacturing industries, numerous attempts have been made to analyze the effect of transverse magnetic field on boundary layer flow characteristics.

2. Mathematical formulation

Consider thermal radiation, chemical reaction, viscous dissipation and Joule heating on a two-dimensional unsteady natural convection flow of electrical magnetohydrodynamic (MHD) nanofluid due to a linearly stretching sheet with suction effect. The velocity of the stretching sheet is denoted as $u_W(x) = bx/1 - at$, where b is the stretching rate and a represent the constant having dimension (time)$^{-1}$ such as $(at < 1, a \geqslant 0)$. The boundary layer equations of the fluid flow are consist of the continuity equation, the momentum equation, energy equation and concentration equation, the flow equation is formulated based on Maxwell's equation, Ohm's law in the presence of electrical Magnetohydrodynamics (MHD). The flow is due to stretching of the sheet from a slot through two equal and opposite force and thermally radiative. Magnetic and electric fields of strength $B = B_0/\sqrt{1-at}$ and $E = E_0/\sqrt{1-at}$ are applied normal to the flow field, such that the magnetic Reynolds number is selected small. The induced magnetic field is smaller to the applied magnetic field. Hence the induced magnetic field is absence for small magnetic Reynolds number. We choose the Cartesian coordinate system such that x is chosen along the stretching sheet and y -axis denotes the normal to the stretching sheet, u and v are the velocity components of the fluid in the x and y -direction see Fig. 1. The two-dimensional natural convection of electrical magnetohydrodynamic (MHD) boundary layer flow equations (Pal and Mondal, 2010; Hayat et al., 2014; Hsiao, 2017; INCLINED, 2003; Mukhopadhyay and Dandapat, 2004):

Continuity equation

$$\frac{\partial u}{\partial x}+\frac{\partial v}{\partial y}=0 \tag{1}$$

$x-$ Momentum equation

$$\frac{\partial u}{\partial t}+u\frac{\partial u}{\partial x}+v\frac{\partial u}{\partial y}=-\frac{1}{\rho_f}\frac{\partial p}{\partial x}+\nu\left(\frac{\partial^2 u}{\partial x^2}+\frac{\partial^2 u}{\partial y^2}\right)+\frac{\sigma}{\rho_f}(EB-B^2u)+\frac{1}{\rho_f}[(1-\varphi_\infty)\rho_{f\infty}\beta_T(T-T_\infty)+(\rho_p-\rho_{f\infty})\beta_\varphi(\varphi-\varphi_\infty)]g \tag{2}$$

$y-$ Momentum equation

$$\frac{\partial v}{\partial t}+u\frac{\partial v}{\partial x}+v\frac{\partial v}{\partial y}=-\frac{1}{\rho_f}\frac{\partial p}{\partial y}+\nu\left(\frac{\partial^2 v}{\partial x^2}+\frac{\partial^2 v}{\partial y^2}\right)+\frac{\sigma}{\rho_f}(EB-B^2v)+\frac{1}{\rho_f}[(1-\varphi_\infty)\rho_{f\infty}\beta_T(T-T_\infty)+(\rho_p-\rho_{f\infty})\beta_\varphi(\varphi-\varphi_\infty)]g \tag{3}$$

Energy equation

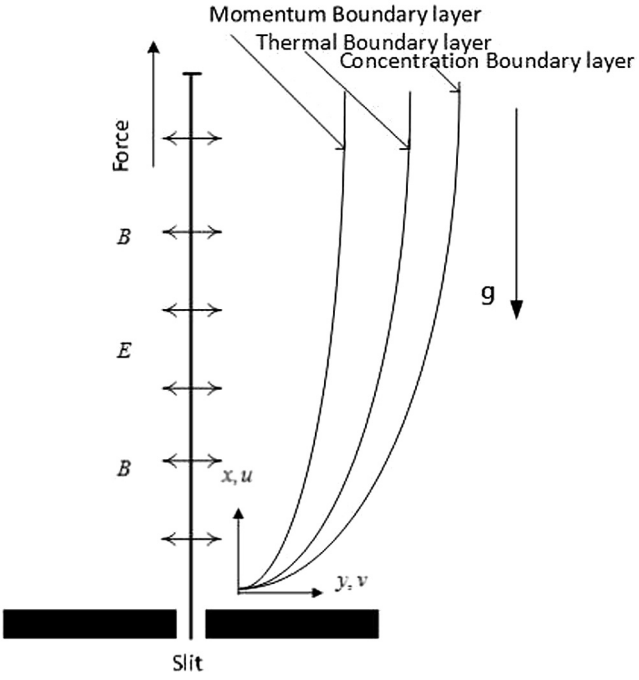

Fig. 1. Physical configuration of the geometry.

$$\frac{\partial T}{\partial t}+u\frac{\partial T}{\partial x}+v\frac{\partial T}{\partial y}=\frac{k}{(\rho c)_f}\left(\frac{\partial^2 T}{\partial x^2}+\frac{\partial^2 T}{\partial y^2}\right)-\frac{1}{(\rho c)_f}\left(\frac{\partial q_r}{\partial y}\right)+\frac{\mu}{(\rho c)_f}\left(\frac{\partial u}{\partial y}\right)^2+\frac{\sigma}{(\rho c)_f}(uB-E)^2+\tau\left\{D_B\left(\frac{\partial \varphi}{\partial x}\frac{\partial T}{\partial x}+\frac{\partial \varphi}{\partial y}\frac{\partial T}{\partial y}\right)+\frac{D_T}{T_\infty}\left[\left(\frac{\partial T}{\partial x}\right)^2+\left(\frac{\partial T}{\partial y}\right)^2\right]\right\} \tag{4}$$

Concentration equation

$$\frac{\partial \varphi}{\partial t}+u\frac{\partial \varphi}{\partial y}+v\frac{\partial \varphi}{\partial y}=D_B\left(\frac{\partial^2 \varphi}{\partial x^2}+\frac{\partial^2 \varphi}{\partial y^2}\right)+\frac{D_T}{T_\infty}\left(\frac{\partial^2 T}{\partial x^2}+\frac{\partial^2 T}{\partial y^2}\right)-k_1(\varphi-\varphi_\infty) \tag{5}$$

The boundary conditions at the sheet for the physical model are presented by

$$y=0:\ u=u_w(x,t),\ \ v=v_w(x,t),\ \ T=T_W(x,t),\ \ D_B\frac{\partial \varphi}{\partial y}+\frac{D_T}{T_\infty}\frac{\partial T}{\partial y}=0$$
$$y\to\infty:\ u\to 0,\ \ T\to T_\infty,\ \ \varphi\to\varphi_\infty \tag{6}$$

The radiative heat flux q_r via Rosseland approximation as discussed in (Daniel and Daniel, 2015) is applied to Eq. (4), such that.

$$q_r=-\frac{4\sigma^*}{3k^*}\frac{\partial T^4}{\partial y} \tag{7}$$

where σ^* represent the Stefan-Boltzmann constant and k^* denote the mean absorption coefficient. Expanding T^4 by using Taylor's series about T_∞ and neglecting higher order terms, we have,

$$T^4\cong 4T_\infty^3T-3T_\infty^4 \tag{8}$$

Using Eq. (8) into Eq. (7), we get

$$\frac{\partial q_r}{\partial y}=-\frac{16T_\infty^3\sigma^*}{3k^*}\frac{\partial^2 T}{\partial y^2} \tag{9}$$

Use Eq. (9) in Eq. (4), we obtain

$$\frac{\partial T}{\partial t}+u\frac{\partial T}{\partial x}+v\frac{\partial T}{\partial y}=\frac{k}{(\rho c)_f}\left(\frac{\partial^2 T}{\partial x^2}+\frac{\partial^2 T}{\partial y^2}\right)+\frac{1}{(\rho c)_f}\left(\frac{16T_\infty^3\sigma^*}{3k^*}\frac{\partial^2 T}{\partial y^2}\right)+\frac{\mu}{(\rho c)_f}\left(\frac{\partial u}{\partial y}\right)^2+\frac{\sigma}{(\rho c)_f}(uB-E)^2+\tau\left\{D_B\left(\frac{\partial\varphi}{\partial x}\frac{\partial T}{\partial x}+\frac{\partial\varphi}{\partial y}\frac{\partial T}{\partial y}\right)+\frac{D_T}{T_\infty}\left[\left(\frac{\partial T}{\partial x}\right)^2+\left(\frac{\partial T}{\partial y}\right)^2\right]\right\} \tag{10}$$

Using the order of magnitude analysis for the y-direction momentum equation which is normal to the stretching sheet and boundary layer approximation (Ibrahim and Shankar, 2013), such as

$$u\gg v,\quad \frac{\partial u}{\partial y}\gg\frac{\partial u}{\partial x},\frac{\partial v}{\partial t},\frac{\partial v}{\partial x},\frac{\partial v}{\partial y},\quad \frac{\partial p}{\partial y}=0 \tag{11}$$

After the analysis, the boundary layer Eqs. (1)–(5) are reduced to the following as:

$$\frac{\partial u}{\partial x}+\frac{\partial v}{\partial y}=0 \tag{12}$$

$$\frac{\partial u}{\partial t}+u\frac{\partial u}{\partial x}+v\frac{\partial u}{\partial y}=-\frac{1}{\rho_f}\frac{\partial p}{\partial x}+\nu\left(\frac{\partial^2 u}{\partial y^2}\right)+\frac{\sigma}{\rho_f}(EB-B^2u)+\frac{1}{\rho_f}\left[(1-\varphi_\infty)\rho_{f\infty}\beta_T(T-T_\infty)+(\rho_p-\rho_{f\infty})\beta_\varphi(\varphi-\varphi_\infty)\right]g \tag{13}$$

$$\frac{\partial T}{\partial t}+u\frac{\partial T}{\partial x}+v\frac{\partial T}{\partial y}=\frac{k}{(\rho c)_f}\left(\frac{\partial^2 T}{\partial y^2}\right)+\frac{1}{(\rho c)_f}\left(\frac{16T_\infty^3\sigma^*}{3k^*}\frac{\partial^2 T}{\partial y^2}\right)+\frac{\mu}{(\rho c)_f}\left(\frac{\partial u}{\partial y}\right)^2+\frac{\sigma}{(\rho c)_f}(uB-E)^2+\tau\left\{D_B\left(\frac{\partial\varphi}{\partial y}\frac{\partial T}{\partial y}\right)+\frac{D_T}{T_\infty}\left(\frac{\partial T}{\partial y}\right)^2\right\} \tag{14}$$

$$\frac{\partial\varphi}{\partial t}+u\frac{\partial\varphi}{\partial y}+v\frac{\partial\varphi}{\partial y}=D_B\left(\frac{\partial^2\varphi}{\partial y^2}\right)+\frac{D_T}{T_\infty}\left(\frac{\partial^2 T}{\partial y^2}\right)-k_1(\varphi-\varphi_\infty) \tag{15}$$

The boundary conditions for the physical model are presented as:

$$y=0:\ u=u_w(x,t),\ v=v_w(x,t),\ T=T_W(x,t),\ D_B\frac{\partial\varphi}{\partial y}+\frac{D_T}{T_\infty}\frac{\partial T}{\partial y}=0$$
$$y\to\infty:\ u\to 0,\ T\to T_\infty,\ \varphi\to\varphi_\infty \tag{16}$$

where $u_w(x,t)=bx/1-at$ denotes the velocity of the linear stretching sheet, $v_w=-v_0/\sqrt{1-at}$ is the wall mass transfer, when $v_w<0$ denote the injection while $v_w>0$ indicates the suction. Where u and v represent the velocity components along the x and y -axis respectively. $p,\alpha=k/(\rho c)_f,\mu,\rho\rho_f$, and ρ_p is for the fluid pressure, the thermal diffusivity, the kinematic viscosity, the density, the fluid density and particles density respectively. We also have $D_B,D_T,\tau=(\rho c)_p/(\rho c)_f$ and $k_1=k_0/(1-at)$ which represents the Brownian diffusion coefficient, the thermophoresis diffusion coefficient, the ratio between the effective heat transfer capacity of the ultrafine nanoparticle material and the heat capacity of the fluid, and the rate of chemical reaction respectively.

Eqs. (12)–(16) are reduced into the dimensionless form by introducing the following suitable dimensionless quantities.

$$\psi=\sqrt{\frac{b\nu}{1-at}}xf(\eta),\quad \eta=y\sqrt{\frac{b}{\nu(1-at)}},\quad \theta=\frac{T-T_\infty}{T_w-T_\infty},\quad \phi=\frac{\varphi-\varphi_\infty}{\varphi_\infty},$$
$$T_w(x,t)=T_\infty+T_0\frac{bx}{2\nu(1-at)^2}, \tag{17}$$

The stream function ψ can be defined as:

$$u=\frac{\partial\psi}{\partial y},\quad v=-\frac{\partial\psi}{\partial x} \tag{18}$$

The equations of momentum, energy and nanoparticle concentration in dimensionless form, after using Eqs. (17) and (18) into Eqs. (12)–(16) become:

$$f'''+ff''-f'^2-\delta\left(f'+\frac{\eta}{2}f''\right)+M(E_1-f')+Gr\theta+Gm\phi=0 \tag{19}$$

$$\frac{1}{Pr}\left(1+\frac{4}{3}Rd\right)\theta''+f\theta'-2f'\theta-\delta\left(\frac{\eta}{2}\theta'+2\theta\right)+Nb\phi'\theta'+Nt\theta'^2+Ec(f'')^2+MEc(f'-E_1)^2=0 \tag{20}$$

$$\phi''+\frac{Nt}{Nb}\theta''+Scf\phi'-Sc\delta\frac{\eta}{2}\phi'-Sc\gamma\phi=0 \tag{21}$$

The boundary conditions are given by

$$f=s,\quad f'=1,\quad \theta=1,\quad Nb\phi'+Nt\theta'=0\quad \text{at } \eta=0$$
$$f'=0,\quad \theta=0,\quad \phi=0,\ \text{as}\ \eta\to\infty \tag{22}$$

where f',θ and ϕ is the dimensionless velocity, temperature, and concentration, respectively, $\delta=a/b$ represent the unsteadiness parameter, $Gr=G_T/Re^2$, where $G_T=g\beta_T(1-\varphi_\infty)(T_w-T_\infty)x^3/\nu^2$ is the Grashof number, $Gm=G_C/Re^2$, where $G_C=g\beta_\varphi(\rho_p-\rho_{f\infty})\varphi_\infty x^3/\nu^2\rho_f$ denotes the mass Grashof number, $Pr=\nu/\alpha$ stand for Prandtl number, $Nb=(\rho c)_pD_B\varphi_\infty/(\rho c)_f\nu$ associates with the Brownian motion parameter, $Sc=\nu/D_B$ is the Schmidt number, $Nt=(\rho c)_pD_T(T_w-T_\infty)/(\rho c)_f\nu T_\infty$ indicates the thermophoresis parameter, $M=\sigma B_0^2/b\rho_f$ is the magnetic field parameter, $E_1=E_0/u_WB_0$ depicts the electric field parameter, $Ec=u_W^2/c_p(T_w-T_\infty)$ is for the Eckert number, $s=v_0/\sqrt{\nu b}$ is the suction parameter and $Rd=4\sigma^*T_\infty^3/k^*k$ stands for the radiation parameter, $\gamma=k_0/b$ is the chemical reaction, for $\gamma>0$ associates to destructive chemical reaction while $\gamma<0$ corresponds to generative chemical reaction respectively. Where prime represents differentiation with respect to η. In our present study, the selection of non-dimensional embedded parameters of nanofluids is considered to vary in view of the works of. The present work is structured in the following aforementioned investigations with water as the base fluid.

The skin friction coefficient and the local Nusselt number are

$$c_f=\frac{\tau_w}{\rho u_w^2(x,t)},\quad Nu=\frac{xq_w}{k(T_w-T_\infty)}, \tag{23}$$

where

$$\tau_w=\mu_f\left(\frac{\partial u}{\partial y}\right)_{y=0},\quad q_w=-\left(\left(k+\frac{16\sigma^*T_\infty^3}{3k^*}\right)\frac{\partial T}{\partial y}\right)_{y=0}, \tag{24}$$

Here τ_w is the shear stress in the stretching surface, q_w is the surface heat flux, $Re=u_wx/\nu$ is the Reynolds number and k is the thermal conductivity of the nanofluid. For the local skin-friction

coefficient and local Nusselt number are presented in non-dimensional form as

$$Re^{1/2}c_f = f''(0), \quad Nu/Re^{1/2} = -\left(1+\frac{4}{3}Rd\right)\theta'(0), \tag{25}$$

3. Results and discussion

The system of nonlinear ordinary differential Eqs. (19)–(21) subjected to the boundary conditions (22) is solved numerically for the diverse values of physical emerging parameters such as magnetic field M, electric field E_1, suction parameter s, Grashof number Gr, mass Grashof number Gm, thermal radiation Rd, Eckert number Ec, unsteadiness parameter δ, Brownian motion parameter Nb, thermophoresis parameter Nt, Schmidt number Sc, and chemical reaction parameter γ. Numerical results were achieved through implicit finite difference scheme known as Keller box method detailed description of the method see (Cebeci & Bradshaw, 2012). For the validation of present numerical scheme, the results are presented and examined with (Ibrahim and Shankar, 2013) in some limiting case when $E_1 = \delta = Gr = Gm = 0$. The numerical values are in good agreement as displayed from Table 1 presents the effects of emerging parameters on the skin friction coefficient.

Fig. 2 render the influence of electric field E_1 and suction s parameters on the dimensionless velocity of nanofluid by keeping other physical parameters constant. Increasing in the suction, the dimensionless velocity reduces in the vicinity of the sheet for the lower values of electric field parameter. For remarkably boost up in the magnitude of the electric field, the resistance between fluid particles increases so that Lorentz force tends to accelerate the body forces and hence leads to increase in the flow of the nanofluid velocity and hence thicker momentum boundary layer. It also resolves sticky effect on the nanoparticles in the fluid. Inside momentum boundary layer, the dimensionless velocity decreases with an increase in the suction and increases with the electric field parameter. In the absence of both suction and magnetic field parameters, the dimensionless velocity in the hydrodynamic boundary layer is found to be larger and it decreases with an increase in the magnetic field and the variation in the suction parameters. The behavior of magnetic field and suction parameters on the nanofluid velocity within the hydrodynamic boundary layer are demonstrations in Fig. 3. In the absence of magnetic field M and suction s, the nanofluid velocity noticed to be higher and decreases with increasing magnetic field and suction parameters. Intense magnetic field influence contributes resistance to flow in the stretching direction. Physically, the outcome of the magnetic field

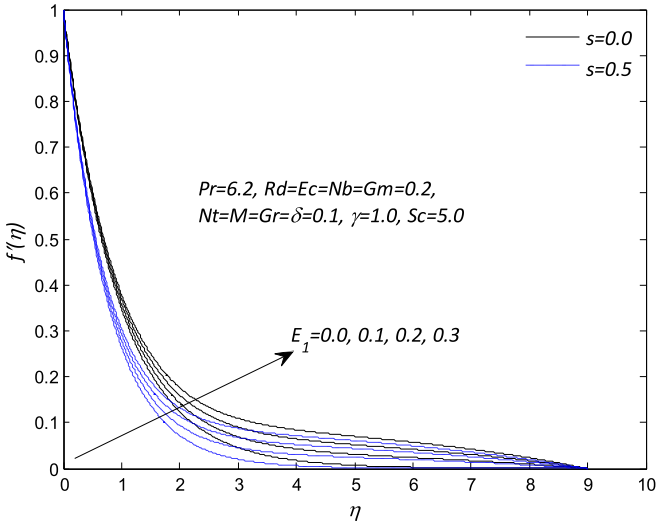

Fig. 2. Influence of E_1 on the velocity profile $f'(\eta)$.

is such that it offers rise to Lorentz force as result of interaction with the electrically conducting nanofluid in a direction which opposes the flow leading to decrease in the velocity. The profiles adhere to the boundary for strong magnetic field indicating that boundary layer thickness is a decreasing function of magnetic field. Fig. 4 elucidates the influence of thermal radiation without and with suction on nanofluid temperature profile. In this figure that the effect of thermal radiation enhances the nanofluid temperature and its associated thermal thickness of the boundary layer to the maximum in the absence of suction. For large values of radiation parameter, generates a significant amount of heating to the nanofluid which enhances the nanofluid temperature profile and thicker thermal boundary layer thickness. The impact of magnetic field M and suction s on the nanofluid temperature profile is a sketch in Fig. 5. It is worth notice that temperature of the nanofluid enhances significantly with increase in the magnetic field without suction. It is interesting to note that increasing magnetic field parameter resistance between fluid particles upsurges, so that heat is created and as a result, the thermal layer becomes thicker and leads to a rise in the temperature of the nanofluid. In Fig. 6 depicts the influence of electric field parameter E_1 and suction s on the nanofluid temperature. It is evident that an increase in the electric field leads to the increment in the temperature profile. Because for higher values of the electric field, Lorentz force accelerated the body forces as results of interaction with the electrically conducting nanofluid yield increases in the temperature of the nanofluid

Table 1
Comparison of Skin friction coefficient $-f''(0)$ when $Gr = Gm = 0$ for various values of M, s, E_1, and δ.

M	s	E_1	δ	Ref (Ibrahim and Shankar, 2013)	Present results
0	0.5	0	0	1.2808	1.280777
0.5				1.5000	1.500000
1.0				1.6861	1.686141
1.5				1.8508	1.850781
2.0				2.0000	2.000000
1.0	0			1.4142	1.414214
	0.2			1.5177	1.517745
	0.7			1.8069	1.806880
	1.0			2.0000	2.000000
	0.2	0.1		–	1.335083
		0.3		–	1.003660
		0.5		–	0.698797
		0.1	0.2	–	1.400699
			0.7	–	1.547543
			1.5	–	1.774626

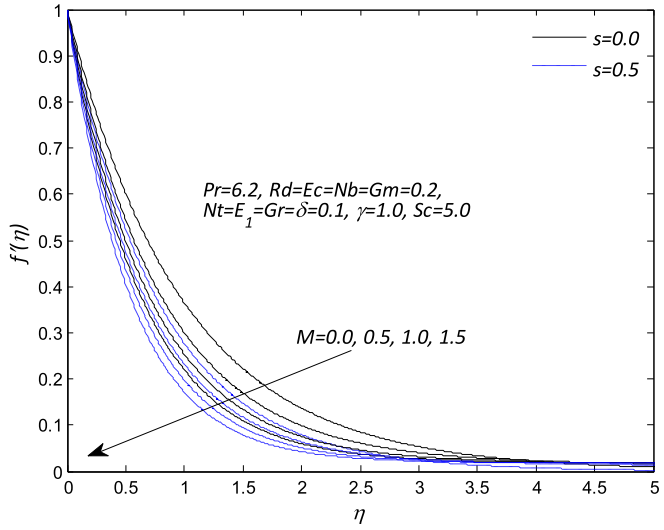

Fig. 3. Influence of M on the velocity profile $f'(\eta)$.

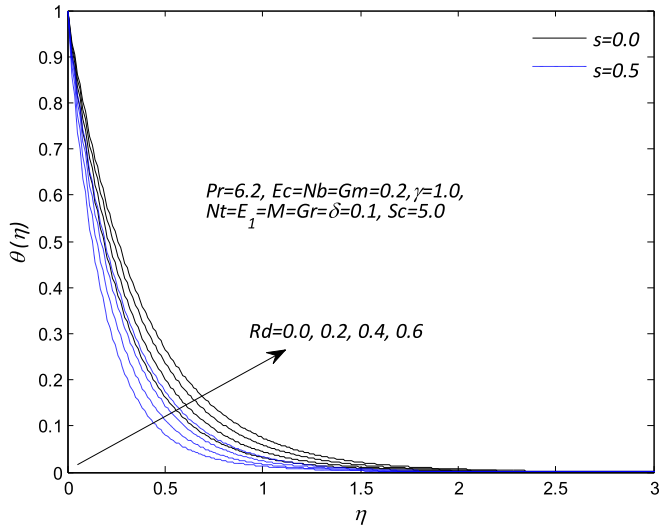

Fig. 4. Influence of Rd on the temperature profile $\theta(\eta)$.

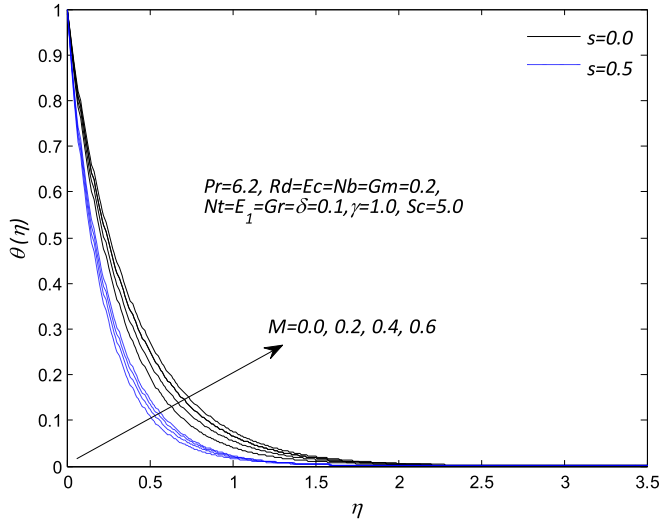

Fig. 5. Influence of M on the temperature profile $\theta(\eta)$.

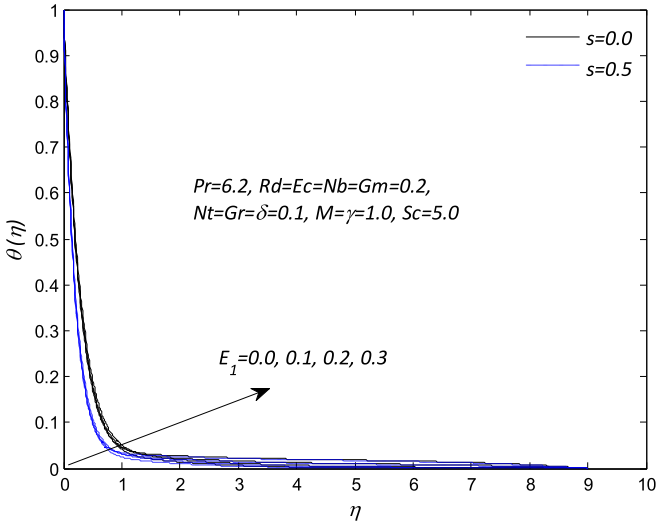

Fig. 6. Influence of E_1 on the temperature profile $\theta(\eta)$.

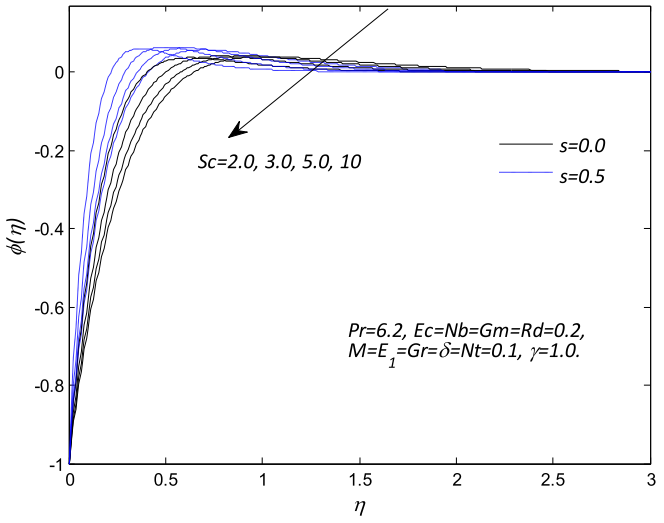

Fig. 7. Influence of Sc on the concentration profile $\phi(\eta)$.

and thicker thermal boundary layer. Fig. 7 reveals the effect of Schmidt number Sc and suction s on the nanoparticle concentration profile. The Schmidt number is the ratio of kinematic viscosity to molecular mass diffusivity for an increase in Schmidt number caused a reduction in mass diffusivity in the system which resulted in a decrease greatly with suction in nanoparticle concentration. The effects of the suction s and chemical reaction γ parameters on the nanoparticles concentration profiles are presented in Fig. 8. It is discerned from this Fig that the concentration profile diminishes with an increase in the chemical reaction and suction parameters. It is also noticed that nanoparticle concentration and layer thickness shrinkage with the destructive chemical reaction. Considerably, the presence of destructive sources the change of the species as a cause of chemical reaction and suction which drops the concentration profiles in the concentration boundary layer thickness.

Fig. 9 elucidates the effects of the suction parameter on the skin friction for different values of magnetic field. It is worthy of note that the suction parameter compliment the skin friction coefficient. Higher values of magnetic field parameter lead to an increment in the skin friction profiles. The reason is that the magnetic field retards the flow of the nanofluid over the stretching sheet sur-

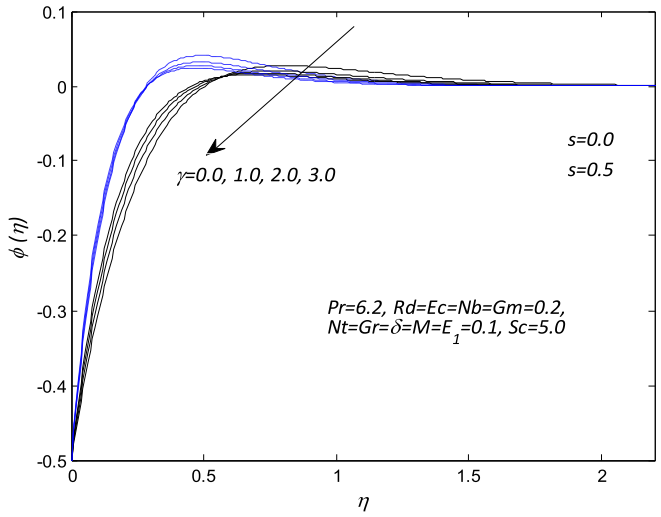

Fig. 8. Influence of γ on the concentration profile $\phi(\eta)$.

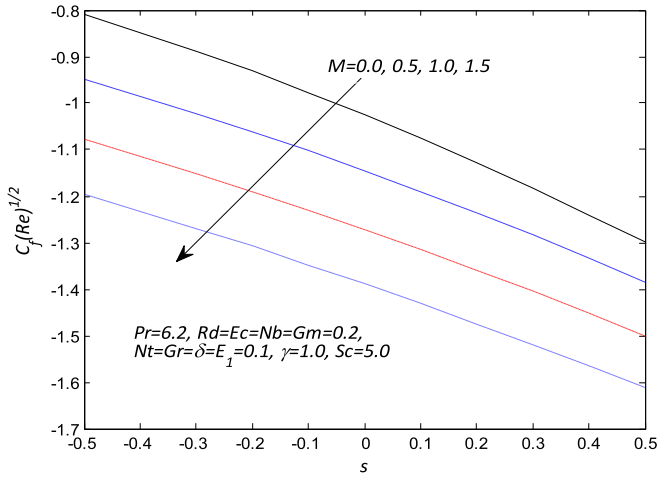

Fig. 9. Influence of M and s on the skin friction $c_f(Re)^{1/2}$.

face due to a stronger hydromagnetic body force which leads to an increase in the skin friction coefficient. However, the injection parameter helps in decreasing the skin friction coefficient. The effects of the electric field and suction/injection parameters on the skin friction profile are portrayed in Fig. 10. It is important to note that both electric field and injection parameters tend to decrease the skin friction. It is interesting to note that increases in an electric field cause Lorenz force to intensify and leads to a substantial flow of the nanofluid due to convection over the sheet surface. Conversely rising in the values of suction parameter caused a rise in the skin friction profile. The influence of the nanofluid parameters via unsteadiness and Brownian motion parameters on the Nusselt number is painted in Fig. 11 for various values. It is imperative to observe that both Brownian motion and unsteadiness parameters yielded to an increase in the profile. So, the Nusselt number increases with augmenting of this parameter. Enhance in the unsteadiness which can be associated with reducing the nanofluid temperature and the thermal layer. In addition, the temperature enhances for the lower acceleration. As the random motion of nanoparticles intensifies, the collision of nanoparticles and kinetic energy rises. Hence, the heat transfer rate on the surface of the sheet increase with an effect of kinetic energy is transformed into heat energy with passively control conditions. Fig. 12 entails the effect of Eckert number and thermophoresis

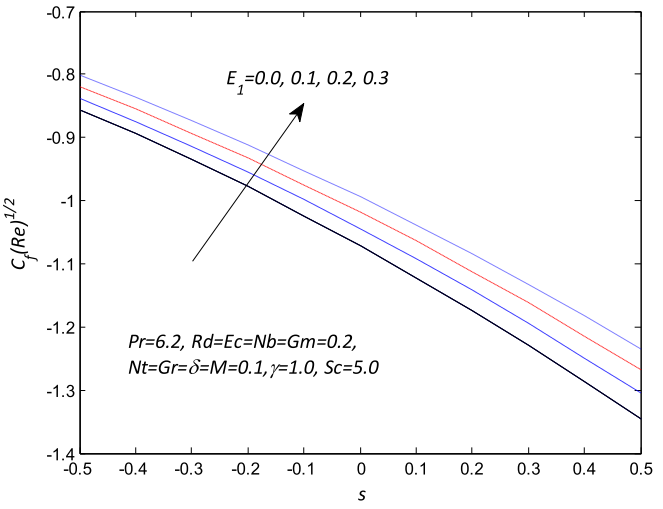

Fig. 10. Influence of E_1 and s on the skin friction $c_f(Re)^{1/2}$.

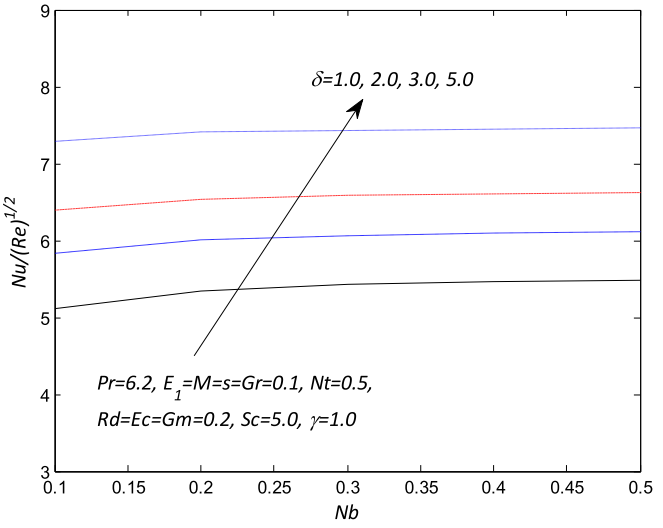

Fig. 11. Influence of δ and Nb on the Nusselt number $Nu/(Re)^{1/2}$.

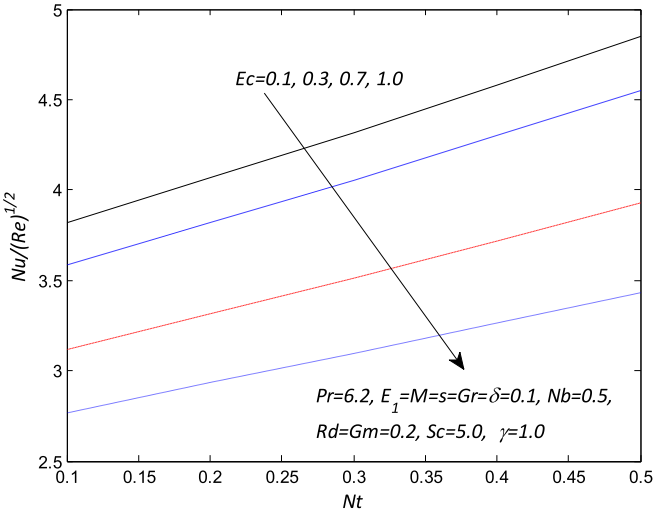

Fig. 12. Influence of Ec and Nt on the Nusselt number $Nu/(Re)^{1/2}$.

parameters on the Nusselt number for different values necessitates. In the presence of suction, the Nusselt number profile is lower with an increase in the Eckert number. As results of the viscosity of fluid gain energy from nanoparticle randomness motion and converts it into internal energy due to which nanofluid temperature is heated. Nonetheless, the thermophoresis parameter tends to increase the profile for higher values.

4. Conclusion

The combined effects of thermal radiation, chemical reaction, viscous dissipation and Joule Heating in a two-dimensional natural convection flow of an electrical MHD nanofluid due to the revised model were discussed in the presence of suction. Main findings of the present study are potted below:

1. Velocity and temperature profiles rise for increment in the values of electric field parameter.
2. It was seen that the Lorentz force due to the presence of magnetic field have a bearing on its resistance to fluid motion and enhances the thermal resistance.
3. Temperature profile shows increasing behavior for larger values of thermal radiation and viscous dissipation. An increase in chemical reaction parameter leads to lower nanoparticles concentration profile.
4. Larger values of suction cause decreasing in velocity, temperature, and nanoparticles concentration distributions.
5. Skin friction for larger values of electric and magnetic fields displayed opposite behavior in the presence of suction/injection.
6. Nusselt number profiles get higher with nanofluid parameter viz Brownian motion and thermophoresis in the presence of unsteadiness parameter.
7. The present results reduce to the steady force convection fluid flow case when $Gr = Gm = \delta = 0$.

Acknowledgments

The authors would like to acknowledge Ministry of Higher Education and Research Management Centre, UTM for the financial support through GUP with vote number 11H90, Flagship grants with vote numbers 03G50 and 03G53 for this research.

References

Ahmed, S.E., Raizah, Z., Aly, A.M., 2019. Entropy generation due to mixed convection over vertical permeable cylinders using nanofluids. J. King Saud Univ.-Sci. 31, 352–361. https://doi.org/10.1016/j.jksus.2017.07.010.

Biglarian, M., Gorji, M.R., Pourmehran, O., Domairry, G., 2017. H_2O based different nanofluids with unsteady condition and an external magnetic field on permeable channel heat transfer. Int. J. Hydrogen Energy. https://doi.org/10.1016/j.ijhydene.2017.07.085.

Buongiorno, J., 2006. Convective transport in nanofluids. J. Heat Transfer 128, 240–250.

Cebeci, T., Bradshaw, P., 2012. Physical and Computational Aspects of Convective Heat Transfer. Springer Science & Business Media.

Choi, S., Eastman, J., 1995. Enhancing thermal conductivity of fluids with nanoparticles. ASME International menchanical engineering congress and exposition. American Society of Mechanical Engineers, San Francisco.

Daniel, Y., 2015a. Presence of heat generation/absorption on boundary layer slip flow of nanofluid over a porous stretching sheet. Am. J. Heat Mass Transfer 2, 15–30.

Daniel, Y.S., 2015b. Presence of heat generation/absorption on boundary layer slip flow of nanofluid over a porous stretching sheet. Am. J. Heat Mass Transfer 2, 15.

Daniel, Y.S., 2015c. Steady MHD laminar flows and heat transfer adjacent to porous stretching sheets using HAM. Am. J. Heat Mass Transfer 2, 146–159.

Daniel, Y.S., 2016a. Laminar convective boundary layer slip flow over a flat plate using homotopy analysis method. J. Inst. Eng. (India): Ser. E 97, 115–121.

Daniel, Y.S., 2016b. Steady MHD boundary-layer slip flow and heat transfer of nanofluid over a convectively heated of a non-linear permeable sheet. J. Adv. Mech. Eng. 3, 1–14.

Daniel, Y.S., Daniel, S.K., 2015. Effects of buoyancy and thermal radiation on MHD flow over a stretching porous sheet using homotopy analysis method. Alexandria Eng. J. 54, 705–712.

Daniel, Y.S., Aziz, Z.A., Ismail, Z., Salah, F., 2017a. Effects of slip and convective conditions on MHD flow of nanofluid over a porous nonlinear stretching/shrinking sheet. Aust. J. Mech. Eng., 1–17

Daniel, Y.S., Aziz, Z.A., Ismail, Z., Salah, F., 2017b. Effects of thermal radiation, viscous and Joule heating on electrical MHD nanofluid with double stratification. Chin. J. Phys. 55, 630–651.

Daniel, Y.S., Aziz, Z.A., Ismail, Z., Salah, F., 2017c. Entropy analysis in electrical magnetohydrodynamic (MHD) flow of nanofluid with effects of thermal radiation, viscous dissipation, and Chemical reaction. Theor. Appl. Mech. Lett. https://doi.org/10.1016/j.taml.2017.06.003.

Daniel, Y.S., Aziz, Z.A., Ismail, Z., Salah, F., 2017d. Impact of thermal radiation on electrical MHD flow of nanofluid over nonlinear stretching sheet with variable thickness. Alexandria Eng. J. https://doi.org/10.1016/j.aej.2017.07.007.

Daniel, Y.S., Aziz, Z.A., Ismail, Z., Salah, F., 2017e. Numerical study of Entropy analysis for electrical unsteady natural magnetohydrodynamic flow of nanofluid and heat transfer. Chin. J. Phys. 55, 1821–1848.

Hayat, T., Shafiq, A., Alsaedi, A., 2014. Effect of Joule heating and thermal radiation in flow of third grade fluid over radiative surface. PLoS ONE 9, e83153.

Hayat, T., Bashir, G., Waqas, M., Alsaedi, A., 2016a. MHD 2D flow of Williamson nanofluid over a nonlinear variable thicked surface with melting heat transfer. J. Mol. Liq. 223, 836–844.

Hayat, T., Bashir, G., Waqas, M., Alsaedi, A., 2016b. MHD flow of Jeffrey liquid due to a nonlinear radially stretched sheet in presence of Newtonian heating. Res. Phys. 6, 817–823.

Hayat, T., Waqas, M., Khan, M.I., Alsaedi, A., 2016c. Analysis of thixotropic nanomaterial in a doubly stratified medium considering magnetic field effects. Int. J. Heat Mass Transfer 102, 1123–1129.

Hayat, T., Waqas, M., Shehzad, S., Alsaedi, A., 2016d. Chemically reactive flow of third grade fluid by an exponentially convected stretching sheet. J. Mol. Liq. 223, 853–860.

Hayat, T., Waqas, M., Shehzad, S., Alsaedi, A., 2016e. A model of solar radiation and Joule heating in magnetohydrodynamic (MHD) convective flow of thixotropic nanofluid. J. Mol. Liq. 215, 704–710.

Hayat, T., Waqas, M., Shehzad, S., Alsaedi, A., 2016f. On 2D stratified flow of an Oldroyd-B fluid with chemical reaction: an application of non-Fourier heat flux theory. J. Mol. Liq. 223, 566–571.

Hayat, T., Waqas, M., Shehzad, S.A., Alsaedi, A., 2016g. On model of Burgers fluid subject to magneto nanoparticles and convective conditions. J. Mol. Liq. 222, 181–187.

Hayat, T., Khan, M.I., Waqas, M., Alsaedi, A., Farooq, M., 2017a. Numerical simulation for melting heat transfer and radiation effects in stagnation point flow of carbon–water nanofluid. Comput. Methods Appl. Mech. Eng. 315, 1011–1024.

Hayat, T., Rashid, M., Imtiaz, M., Alsaedi, A., 2017b. MHD effects on a thermo-solutal stratified nanofluid flow on an exponentially radiating stretching sheet. J. Appl. Mech. Tech. Phys. 58, 214–223.

Hayat, T., Waqas, M., Alsaedi, A., Bashir, G., Alzahrani, F., 2017c. Magnetohydrodynamic (MHD) stretched flow of tangent hyperbolic nanoliquid with variable thickness. J. Mol. Liq. 229, 178–184.

Hayat, T., Waqas, M., Khan, M.I., Alsaedi, A., 2017d. Impacts of constructive and destructive chemical reactions in magnetohydrodynamic (MHD) flow of Jeffrey liquid due to nonlinear radially stretched surface. J. Mol. Liq. 225, 302–310.

Hayat, T., Waqas, M., Khan, M.I., Alsaedi, A., Shehzad, S., 2017e. Magnetohydrodynamic flow of burgers fluid with heat source and power law heat flux. Chin. J. Phys. 55, 318–330.

Hayat, T., Zubair, M., Waqas, M., Alsaedi, A., Ayub, M., 2017f. Impact of variable thermal conductivity in doubly stratified chemically reactive flow subject to non-Fourier heat flux theory. J. Mol. Liq. 234, 444–451.

Hayat, T., Zubair, M., Waqas, M., Alsaedi, A., Ayub, M., 2017g. Importance of chemical reactions in flow of Walter-B liquid subject to non-Fourier flux modeling. J. Mol. Liq. 238, 229–235.

Hayat, T., Zubair, M., Waqas, M., Alsaedi, A., Ayub, M., 2017h. On doubly stratified chemically reactive flow of Powell-Eyring liquid subject to non-Fourier heat flux theory. Res. Phys. 7, 99–106.

Hsiao, K.-L., 2016. Stagnation electrical MHD nanofluid mixed convection with slip boundary on a stretching sheet. Appl. Therm. Eng. 98, 850–861.

Hsiao, K.-L., 2017. Combined electrical MHD heat transfer thermal extrusion system using Maxwell fluid with radiative and viscous dissipation effects. Appl. Therm. Eng. 112, 1281–1288.

Ibrahim, W., Makinde, O., 2016. Magnetohydrodynamic stagnation point flow of a power-law nanofluid towards a convectively heated stretching sheet with slip. Proc. Inst. Mech. Eng. Part E 230, 345–354.

Ibrahim, W., Shankar, B., 2013. MHD boundary layer flow and heat transfer of a nanofluid past a permeable stretching sheet with velocity, thermal and solutal slip boundary conditions. Comput. Fluids 75, 1–10.

INCLINED, C.F.F.D.A., 2003. Finite amplitude long wave instability of a film of conducting fluid flowing down an inclined plane in presence of electromagnetic field. Int. J. Appl. Mech. Eng. 8, 379–383.

Kasaeian, A., Azarian, R.D., Mahian, O., Kolsi, L., Chamkha, A.J., Wongwises, S., Pop, I., 2017. Nanofluid flow and heat transfer in porous media: a review of the latest developments. Int. J. Heat Mass Transfer 107, 778–791.

Khan, M., Azam, M., 2017. Unsteady heat and mass transfer mechanisms in MHD Carreau nanofluid flow. J. Mol. Liq. 225, 554–562.

Khan, W., Makinde, O., Khan, Z., 2016. Non-aligned MHD stagnation point flow of variable viscosity nanofluids past a stretching sheet with radiative heat. Int. J. Heat Mass Transfer 96, 525–534.
Khan, M.I., Khan, M.I., Waqas, M., Hayat, T., Alsaedi, A., 2017a. Chemically reactive flow of Maxwell liquid due to variable thicked surface. Int. Commun. Heat Mass Transfer 86, 231–238.
Khan, M.I., Waqas, M., Hayat, T., Alsaedi, A., 2017b. A comparative study of Casson fluid with homogeneous-heterogeneous reactions. J. Colloid Interface Sci. 498, 85–90.
Khan, M.I., Waqas, M., Hayat, T., Khan, M.I., Alsaedi, A., 2017c. Behavior of stratification phenomenon in flow of Maxwell nanomaterial with motile gyrotactic microorganisms in the presence of magnetic field. Int. J. Mech. Sci. 131, 426–434.
Kuznetsov, A., Nield, D., 2013. The Cheng-Minkowycz problem for natural convective boundary layer flow in a porous medium saturated by a nanofluid: a revised model. Int. J. Heat Mass Transfer 65, 682–685.
Mabood, F., Khan, W., Ismail, A.M., 2015. MHD boundary layer flow and heat transfer of nanofluids over a nonlinear stretching sheet: a numerical study. J. Magn. Magn. Mater. 374, 569–576.
Makinde, O., Animasaun, I., 2016. Thermophoresis and Brownian motion effects on MHD bioconvection of nanofluid with nonlinear thermal radiation and quartic chemical reaction past an upper horizontal surface of a paraboloid of revolution. J. Mol. Liq. 221, 733–743.
Makinde, O., Mabood, F., Khan, W., Tshehla, M., 2016. MHD flow of a variable viscosity nanofluid over a radially stretching convective surface with radiative heat. J. Mol. Liq. 219, 624–630.
Makinde, O., Khan, W., Khan, Z., 2017. Stagnation point flow of MHD chemically reacting nanofluid over a stretching convective surface with slip and radiative heat. Proc. Inst. Mech. Eng. Part E 231, 695–703.
Mukhopadhyay, A., Dandapat, B., 2004. Nonlinear stability of conducting viscous film flowing down an inclined plane at moderate Reynolds number in the presence of a uniform normal electric field. J. Phys. D Appl. Phys. 38, 138.
Nayak, M., Akbar, N.S., Pandey, V., Khan, Z.H., Tripathi, D., 2017. 3D free convective MHD flow of nanofluid over permeable linear stretching sheet with thermal radiation. Powder Technol. 315, 205–215.
Pal, D., Mandal, G., 2017. Thermal radiation and MHD effects on boundary layer flow of micropolar nanofluid past a stretching sheet with non-uniform heat source/sink. Int. J. Mech. Sci. 126, 308–318.
Pal, D., Mondal, H., 2010. Hydromagnetic non-Darcy flow and heat transfer over a stretching sheet in the presence of thermal radiation and Ohmic dissipation. Commun. Nonlinear Sci. Numer. Simul. 15, 1197–1209.
Pontes, F.A., Miyagawa, H.K., Pontes, P.C., Macêdo, E.N., Quaresma, J.N., 2019. Integral transform solution of micropolar magnetohydrodynamic oscillatory flow with heat and mass transfer over a plate in a porous medium subjected to chemical reactions. J. King Saud Univ.-Sci. 31, 114–126. https://doi.org/10.1016/j.jksus.2017.07.002.
Sharma, G., Kumar, A., Sharma, S., Naushad, M., Dwivedi, R.P., ALOthman, Z.A., Mola, G.T., 2019. Novel development of nanoparticles to bimetallic nanoparticles and their composites: a review. J. King Saud Univ.-Sci. 31, 257–269. https://doi.org/10.1016/j.jksus.2017.06.012.
Sheikholeslami, M., 2017. Numerical investigation of MHD nanofluid free convective heat transfer in a porous tilted enclosure. Eng. Computations. https://doi.org/10.1108/EC-08-2016-0293.
Sheikholeslami, M., Ganji, D., 2017. Transportation of MHD nanofluid free convection in a porous semi annulus using numerical approach. Chem. Phys. Lett. 669, 202–210.
Sheikholeslami, M., Rokni, H.B., 2017. Magnetic nanofluid natural convection in the presence of thermal radiation considering variable viscosity. Eur. Phys. J. Plus 132, 238.
Sheikholeslami, M., Shamlooei, M., 2017. Fe_3O_4–H_2O nanofluid natural convection in presence of thermal radiation. Int. J. Hydrogen Energy 42, 5708–5718.
Sheikholeslami, M., Shehzad, S., 2017. Thermal radiation of ferrofluid in existence of Lorentz forces considering variable viscosity. Int. J. Heat Mass Transfer 109, 82–92.
Sheikholeslami, M., Hayat, T., Alsaedi, A., 2016. MHD free convection of Al_2O_3–water nanofluid considering thermal radiation: a numerical study. Int. J. Heat Mass Transfer 96, 513–524.
Sheremet, M.A., Oztop, H., Pop, I., 2016. MHD natural convection in an inclined wavy cavity with corner heater filled with a nanofluid. J. Magn. Magn. Mater. 416, 37–47.
Tamoor, M., Waqas, M., Khan, M.I., Alsaedi, A., Hayat, T., 2017. Magnetohydrodynamic flow of Casson fluid over a stretching cylinder. Res. Phys. 7, 498–502.
Ullah, I., Shafie, S., Makinde, O.D., Khan, I., 2017. Unsteady MHD Falkner-Skan flow of Casson nanofluid with generative/destructive chemical reaction. Chem. Eng. Sci. https://doi.org/10.1016/j.ces.2017.07.011.
Waqas, M., Farooq, M., Khan, M.I., Alsaedi, A., Hayat, T., Yasmeen, T., 2016. Magnetohydrodynamic (MHD) mixed convection flow of micropolar liquid due to nonlinear stretched sheet with convective condition. Int. J. Heat Mass Transfer 102, 766–772.
Waqas, M., Khan, M.I., Hayat, T., Alsaedi, A., 2017. Numerical simulation for magneto Carreau nanofluid model with thermal radiation: a revised model. Comput. Methods Appl. Mech. Eng. 324, 640–653.